Crystallization behavior of ternary γ–γ′ Co–Al–W alloy

Damian Migas[1] · Paweł Gradoń[1] · Tomasz Mikuszewski[1] · Grzegorz Moskal[1]

Abstract

In the investigation, crystallization behavior of ternary γ–γ′ alloy based on Co–Al–W system was analyzed. The alloy with nominal composition Co–9Al–9W (at.%) was prepared via vacuum induction melting. Solidification characteristics of the investigated superalloy were obtained by a method of thermal analysis based on temperature measurement of metal solidifying in a mold. After casting, obtained metallic materials were investigated by differential thermal analysis in order to determine characteristic temperatures and compare results with those of obtained in the first thermal analysis. Furthermore, a description of primary microstructure was performed for ingots solidified with two different cooling rates. The analysis was made using X-ray diffraction, optical microscopy and scanning electron microscopy. The crystallization path of alloy was investigated. The solidification range of alloy was narrow. The crystallization in a sand mold resulted in the dendritic microstructure containing γ single phase. The as-cast microstructure after solidification with higher cooling rate was comparable; however, observed crystals were mostly columnar, while sand cast was characterized by equiaxed crystals structure.

Keywords γ–γ′ cobalt-based superalloys · Co–Al–W superalloy · Solidification path · Segregation · Dendrite core · Solidification microstructure

Introduction

The ternary alloys based on Co–Al–W system were the starting point in the development of new group of superalloys strengthened by γ′ phase. For the first time, presence of an ordered $L1_2$ phase in this system was mentioned by Lee [1]. Sato et al. [2] reported existence of a stable γ′-Co_3(Al, W) phase. The γ′ phase is efficient in view of high-temperature strengthening due to very low lattice misfit [2]. Owing to strengthening of ordered $L1_2$ compounds, alloys are characterized by superior high-temperature strength compared to those of conventional Co-based superalloys, which are strengthened by carbides precipitation. This qualitative difference gave possibility for further development of superalloys based on Co. The addition of alloying elements, e.g., Ni, Ta, Ti, Nb, may stabilize the $L1_2$ phase toward higher temperatures [3–6]. Substantial effort was done in order to investigate the role of alloying elements in a microstructure

and properties of new superalloys [7–11]. Relatively low attention was paid to technological aspects.

Most authors focused on manufacturing of alloys on a laboratory scale. Many of them use vacuum arc melting to produce small ingots, dedicated for advanced microstructural researches and other tests. McDevitt [12] produced 22 kg heats of three Co-based superalloys: Co–9Al–9W, Co–9Al–10W–2Ti and Co–9Al–10W–2Ti–0.02B (at.%) by vacuum induction melting (VIM) and vacuum arc remelting (VAR), and then, the alloys were open-die forged. The ingot microstructure of prepared materials was characterized as well as hot workability during billetizing. The author proved that VIM/VAR ingot production is viable for scale up to commercial production and there is a promise for producing large diameter ingots with acceptable segregation. The forging aspects of new Co-based superalloys were further investigated by other scientists [13]. In 2015, Koßman et al. [14] characterized the microsegregation and solidification of a multi-component Co-based superalloy and compared it to a ternary Co–Al–W alloy and to two Ni-based superalloys. Zhou et al. [15] investigated the effect of Ta and Ti on the directional solidification characteristics of novel γ–γ′ Co-based superalloys. The same authors published the work concerning effect of Al and W contents on the solidification

✉ Damian Migas
  damian.migas@polsl.pl

1 Department of Advanced Materials and Technologies, Faculty of Materials Engineering, Silesian University of Technology, Katowice, Poland

and solution microstructure of new cobalt superalloys [16]. Sani et al. [17] performed the research on effect of homogenization heat treatment on segregation and microstructure of γ–γ′ Co-based superalloys. The heat treatment aspects of ternary Co–Al–W alloys were investigation by Tomaszewska et al. [18]. Except arc melting and VIM/VAR methods, works concerning directional solidification [15, 16, 19] and a single crystal solidification [20] of γ′-strengthened Co-based superalloys are available.

The intention of authors is increase in the literature data concerning technological aspects of γ/γ′ Co-based superalloys. The scientific goal of the work is characterization of crystallization behavior of a ternary Co–Al–W alloy under different cooling conditions, including slow cooling, which was not analyzed in the previous studies. The formation of desirable microstructure free of detrimental phases and segregation, upon low cooling rate, is important taking into account manufacturing of greater components. Such casting products are characterized by a longer time of solidification due to a higher thickness. The studies concerning solidification of the Co-based alloys were limited to microstructural aspects. Moreover, from technological point of view, it is important to characterize the temperature window between *liquidus* and *solidus* temperatures. In the case of DSC or DTA analysis of Co–Al–W alloys, there is no distinct effect on cooling curve that may be attributed to crystallization finish. Therefore, in this article, except differential thermal analysis, the characterization of solidification was improved by another method of thermal analysis, which allows to directly characterize thermal behavior of alloy during crystallization in a mold.

Materials and methods

The Co–Al–W alloy with nominal composition Co–9Al–9W (at.%) was prepared by vacuum induction melting in the VSG 02 Balzers furnace. In this process, pure metals including Co, Al and W were used as a feedstock. The alloys were melted in the temperature range 1600–1700 °C for a time of approximately 10 min. The investigated alloys were casted under argon into two types of molds in order to vary cooling rate. The first one, sand mold, was selected due to high isolation properties. This mold was made of CO_2-hardened silica sand. The second mold was made of graphite in order to provide conditions of fast heat dissipation in a solidifying alloy. For obtainment of solidification curves, an appropriate experimental set was developed (Fig. 1). During solidification of the alloy, temperature was recorded via thermocouple (PtRh10-Pt) fit in the sand mold. The thermocouple wires of ø0.5 mm were put in alumina shield. The wires in alumina were additionally fit in quartz tube, which was placed inside the mold. The obtained signal was recorded with a step of 0.5 s by the temperature recorder Crystaldigraph PC-8T connected to a computer. The experimental set including mold and thermocouple was placed inside the furnace chamber. The crystallization curve for alloy solidified in cold graphite mold was not recorded due to very fast crystallization (up to 10 s).

After casting, the thermal analysis including differential thermal analysis (DTA) was carried out on the as-cast specimens. The DTA analysis was carried out using the NETZSCH STA 449 F3 Jupiter device. The temperature range of analysis was 40–1500 °C, whereas the heating and cooling rate was 20 °C min⁻¹. An empty alumina crucible was used as a reference.

The microstructure in as-solidified state was analyzed by optical microscopy (OM), scanning electron microscopy (SEM) and X-ray diffraction (XRD). The optical

Fig. 1 Schematic and real experimental set for registration of crystallization curves

Schematic of experimental set

Real experimental set
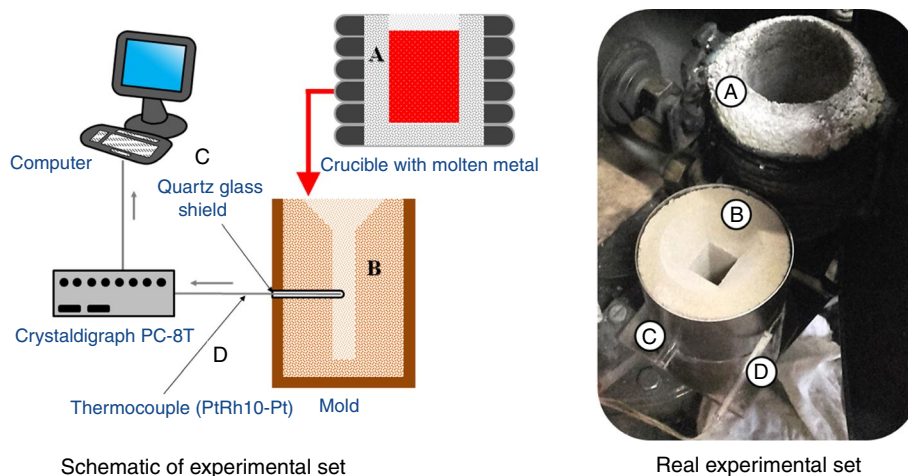
micrographs were carried out using the Nikon Eclipse MA200 light microscope. In the case of SEM/EDS analysis, the scanning electron microscope (SEM, Hitachi S-3400N) equipped with the energy dispersion spectrometer (EDS, Thermo Noran System Seven) was used. The SEM images were captured with the use of backscattered electron (BSE) mode. The phase composition was evaluated using the Phillips X'Pert³ Powder diffractometer. A chemical etching of specimens in solution containing 25 mL H_2O, 50 mL HCl, 15 g $FeCl_3$ and 3 g $CuCl_2 \times NH_4Cl \times 2H_2O$ was used in order to reveal a primary microstructure of as-cast specimens.

Results and discussion

The first part of work concerns thermal analysis of the solidification of a ternary Co–Al–W alloy. The cooling curve and its derivative are shown in Fig. 2. The molten metal contacted thermocouple at temperature slightly higher than 1600 °C. The temperature rapidly decreased down to 1450 °C. At this temperature, the plateau effect may be observed on solidification plot. The measured temperature is constant due to crystallization heat. After about 80 s of solidification, an isothermal section of the plot ends which is also indicated on the derivative curve with the local minimum. Temperature of 1395 °C corresponding to this minimum can be interpreted as solidus temperature. Below 1395 °C, the plot changed its character to typical for cooling without any considerable thermal effects in solid state. The course of cooling curve implies that only one phase crystallized during solidification. Taking into account the literature data concerning these alloys, this phase should be γ-Co_{ss}. Therefore, the solidification path should be as follows: $L \rightarrow L_1 + \gamma \rightarrow \gamma$. Afterward, a microstructural evaluation was performed for the analyzed material.

Figure 3a shows the final ingot whose solidification was analyzed by thermal analysis (Fig. 2). The size of cuboidal ingot was $20 \times 20 \times 100$ mm. Figure 3b, c, d shows macrostructure of the ingot in the plane perpendicular to the ingot axis. The specimens were cut from different parts of the cast. Moreover, Fig. 3e shows macrostructure of the middle part of the ingot in the plane parallel to the ingot axis. All macrographs show coarse crystals primary microstructure. The size of crystals in primary microstructure is several hundred micrometer, and dendrites can be easily observed by unaided eye. The crystals are characterized by randomly oriented dendrite structures. There is a lack of elongated crystals zone. In the case of specimen from the bottom part of cast (Fig. 3d), the size of crystals is slightly lower compared to that of other parts of the cast. It can be connected with the fact that in this area, the heat dissipation occurred faster compared to that of upper parts.

The microstructural evaluation of the obtained as-cast Co–W superalloy may be seen in Fig. 4. The images show microstructure of upper (Fig. 4a, d, g), middle (Fig. 4b, e) and lower (Fig. 4c, f) parts of the ingot. The optical micrographs and SEM micrographs confirm great size of both crystals and dendrites. In the case of crystals, the observable range of size is from few hundred micrometer to few millimeter. The dendrite cells may measure even more than 100 micrometer. The OM micrographs (Fig. 4a–c) revealed grain boundaries. Moreover, SEM micrographs (in this case, specimens were not etched) performed using BSE imaging did not show any substantial changes in color contrast that implies relatively low degree of segregation (Fig. 4d–g). The interdendritic zones are darker that imply some differences in chemical composition; the interdendritic areas are very thin. The element which segregates to interdendritic spaces is Al. However, the measurement of chemical composition in micro-areas in upper part of ingot (Fig. 4g) showed that differences between dendrites and interdendritic areas are very low. The amount of Al in dendrites was about 2 at.% lower compared to that of interdendritic areas (Fig. 4g). The similar results were obtained in lower parts of the ingot.

Another step of investigation was differential thermal analysis (DTA). The appropriate specimen of rectangular shape was cut from the middle part of the ingot. The results of DTA measurements in the temperature range 40–1500 °C are shown in Fig. 5. The heating curve showed a first distinct
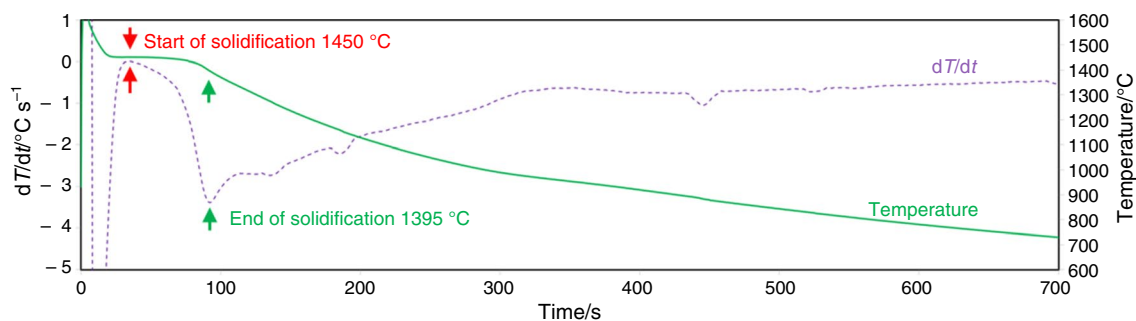

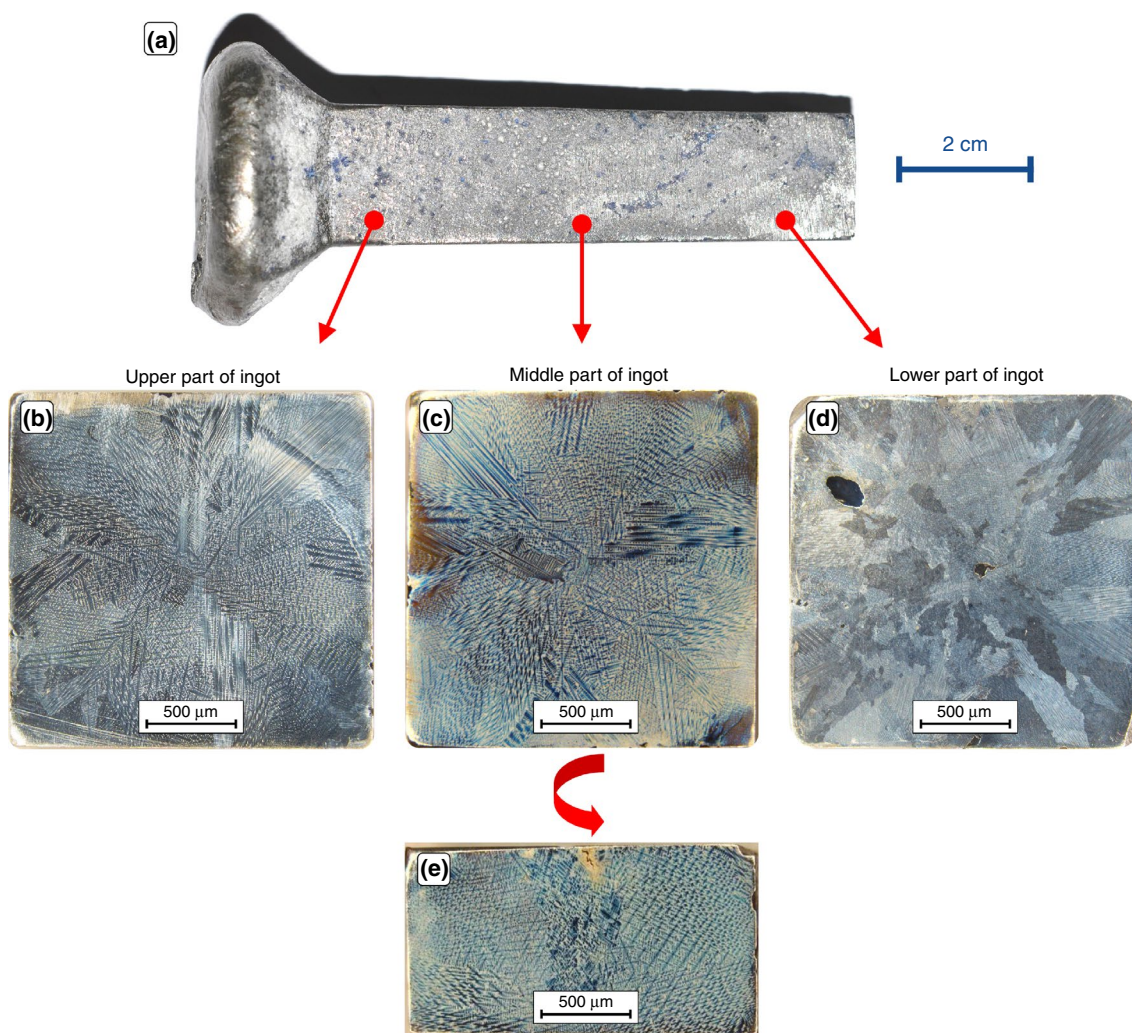**Fig. 2** Crystallization curve of Co–9Al–9W alloy solidified in sand mold

Fig. 3 Macrostructure of ingot solidified in sand mold

thermal effect at 977 °C, which is connected with order–disorder transition of γ' phase. The shape of this individual thermal effect is a characteristic of order–disorder transition [21–23]. This observation showed that chemical composition obtained in as-cast state allows for formation of γ' precipitates. Further heating of alloy did not show any relevant peaks till temperature 1444 °C, which is related to start of melting, according to a character of endothermic peak. Another distinct effect was observed on cooling curve at 1468 °C. At this temperature, considerable exothermic peak occurred and is connected with the start of crystallization (*liquidus* temperature). The maximum of this peak is related to temperature 1425, whereas the end of effect is roughly 1390 °C. The character of cooling curve is adequate to the cooling curve obtained via the first, simple thermal analysis measurement (Fig. 2). The slight differences in values of characteristic points (mainly *liquidus*) may be connected with different cooling rate in both discussed cases.

There was no other thermal effects on cooling curve except the one occurred at 974 °C. This phenomenon is connected with disorder–order transition concomitant precipitation of γ' phase.

The temperatures of thermal effects related with solidification of alloys are comparable to those of observed in the first thermal analysis (Fig. 2). The small differences may be connected to differences in cooling rate. Moreover, in the DTA method, only certain small section of ingot was analyzed, while crystallization curves were captured during solidification of whole ingot. Similar to the first thermal analysis (Fig. 2), DTA analysis did not reveal any additional effects except the start and end of γ phase crystallization. Relatively narrow solidification range and lack of additional effects imply that in this system, only one phase (solid solution of Al and W in Co) is being crystallized from liquid phase. The X-ray diffraction pattern of as-cast alloy (Fig. 6) shows occurrence of only one phase within the primary
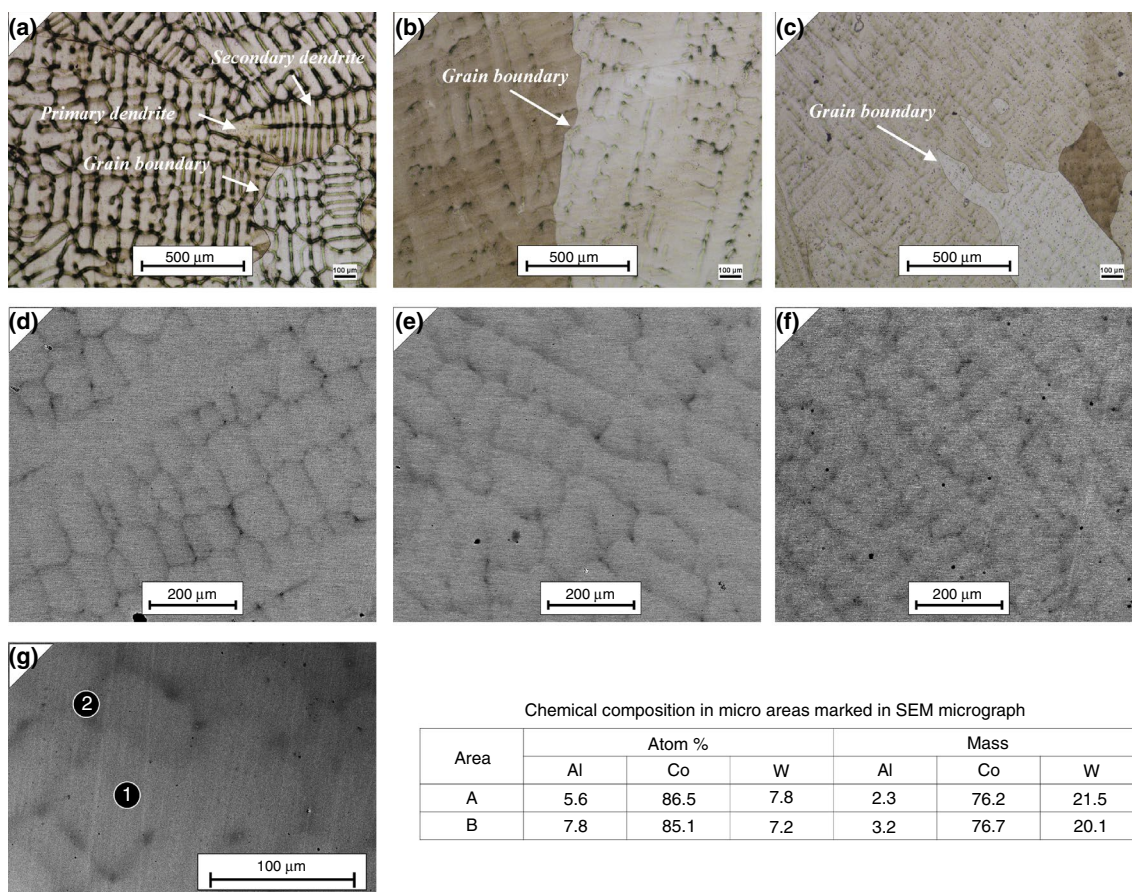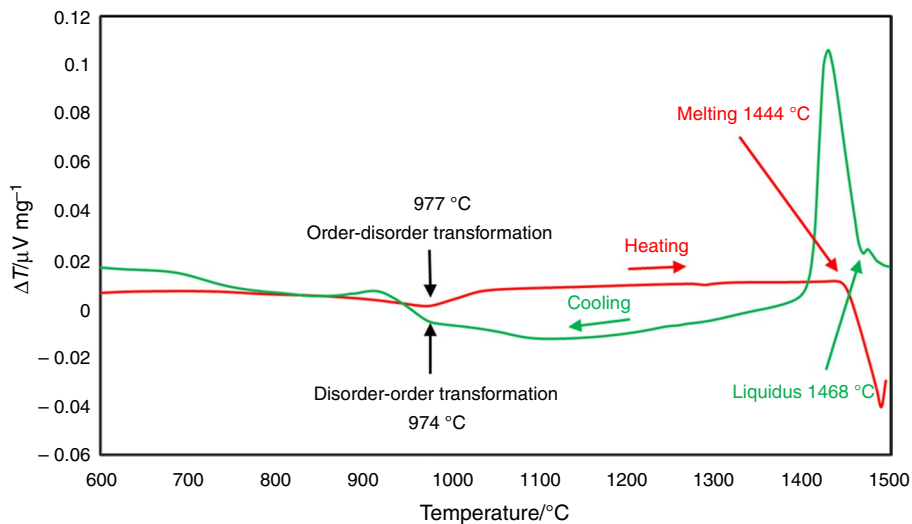
Chemical composition in micro areas marked in SEM micrograph

Area	Atom %			Mass		
	Al	Co	W	Al	Co	W
A	5.6	86.5	7.8	2.3	76.2	21.5
B	7.8	85.1	7.2	3.2	76.7	20.1

Fig. 4 OM and SEM micrographs of primary microstructure of Co–9Al–9W alloy solidified in sand mold

Fig. 5 DTA curves of sand cast made of Co–9Al–9W alloy

microstructure. The only detected phase was cobalt (JCPDS no. 15-0806), which could be attributed to the solid solution of Al and W in cobalt (γ-Co$_{ss}$). No detrimental phases were recognized. Taking into account the high-temperature Co–Al–W system [2, 24], phases such as γ-Co, γ′-Co$_3$(Al, W), β-CoAl, μ-Co$_7$W$_6$ and Co$_3$W may occur. For alloy with nominal composition Co–9Al–9W (at.%), dual-phase γ–γ′ microstructure is expected. Although XRD pattern showed only peaks corresponding to Co, this method cannot exclude occurrence of γ′ phase. Peaks corresponding to γ and γ′ are
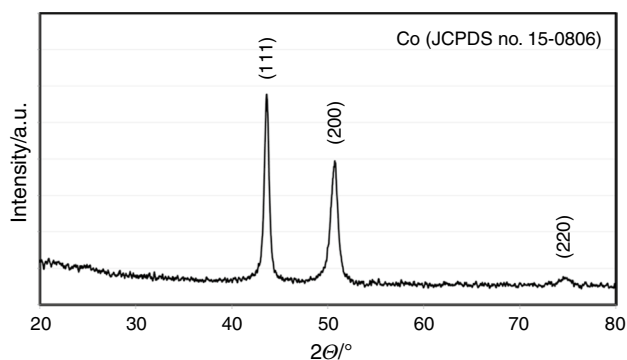
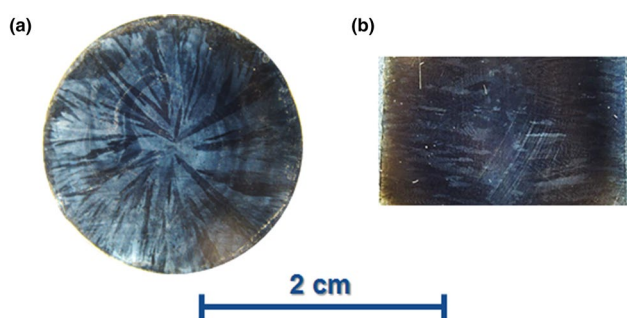**Fig. 6** X-ray diffraction pattern Co–9Al–9W alloy solidified in sand mold

Fig. 7 Macrostructure Co–9Al–9W alloy solidified in graphite mold

practically indistinguishable due to very low lattice misfit [2]. Although microstructural analysis did not exhibit γ' phase in the as-cast state, DTA analysis showed γ' dissolution clearly. Relatively long time of heating from room temperature to 977 °C gave possibility to precipitate γ'; therefore, disordering of this phase can be easily observed on heating curve.

Except analysis of sand cast made of Co-based superalloy, the authors analyzed crystallization behavior of the same alloy obtained via rapid crystallization in a graphite mold. The size of obtained cylindrical ingot was $\varnothing 20 \times 150$ mm. The differential thermal analysis was performed under analogue conditions compared to that of sand mold. The course of DTA curve was almost the same. Moreover, X-ray diffraction analysis showed that single-phase structure (γ solid solution) was obtained in this case. Figure 7 shows macrographs of Co–9Al–9W (at.%) alloy solidified under fast cooling condition. The image that reveals macrostructure in the plane perpendicular to the ingot axis (Fig. 7a) shows elongated crystals that are typical for crystallization with intensive heat dissipation. The view in the plane parallel to the ingot axis (Fig. 7b) revealed that near the axis of ingot, some thin zone of equiaxed crystals may be observable;

however, columnar crystals are dominant within primary microstructure.

The characteristic zones in the as-cast alloy may be easily observed in the OM micrographs (Fig. 8). The low-magnification micrograph (Fig. 8a) shows occurrence of three zones. The zone of equiaxed crystals ("A") is roughly 5 mm in diameter and is located in the middle of the cast. The second zone ("B"), zone of columnar crystals, is substantially greater compared to that of other zones. Other figures (Fig. 8b, c) show the characteristic zones in higher magnification. The last characteristic area is zone of frozen crystals ("C") with thickness of roughly few hundred micrometer. This type of crystals occurs in the outer parts of ingot, where a heat dissipation is the most intensive. In view of plastic working, the primary microstructure obtained under conditions of fast cooling is unfavorable due to high content of columnar crystals. Such problem did not occur in the case of alloy solidified with lower cooling rate (Fig. 9). In this case, the microstructure in the middle of the ingot does not differ substantially compared to the outer zone of the cast. The cross section shows occurrence of only one, equiaxed crystals zone in the both middle (Fig. 9c) and edge of the cross section (Fig. 9b).

Although in the case of ternary Co–Al–W alloy, a fast cooling rate caused formation of numerous elongated crystals, this type of solidification has also advantages, e.g., possible obtainment of supersaturated solid solution. Except columnar crystals, the basic difference between two types of castings is size of crystals and dendritic structures, which is substantially lower in the case of alloy solidified in a mold made of graphite.

Figure 10 shows the SEM micrograph of Co–Al–W alloy solidified in cold graphite mold. Figure 10a shows area of equiaxed crystals. The differences in chemical composition between dendrites and interdendritic zones are low (Fig. 10b). Although microstructure of Co–Al–W sand cast was characterized by relatively low segregation level, the thickness of interdendritic space was at least two times higher compared to that of alloy solidified in graphite mold. Due to low segregation, thin interdendritic areas and supersaturation upon fast cooling, such castings can be then homogenized easily.

The aim of the work was obtained. The solidification of Co–Al–W alloys under different cooling conditions was compared. In the previous investigations, only crystallization under very fast heat dissipation was considered. Such type of crystallization occurs mostly in the case of thin-walled components. Taking into account the casting of greater elements, an increase in the component's size changes the crystallization conditions by slower solidification rate. In the investigations, such casting conditions were simulated using sand mold, which elongated time of crystallization time of the ingot. The results showed that this increase did
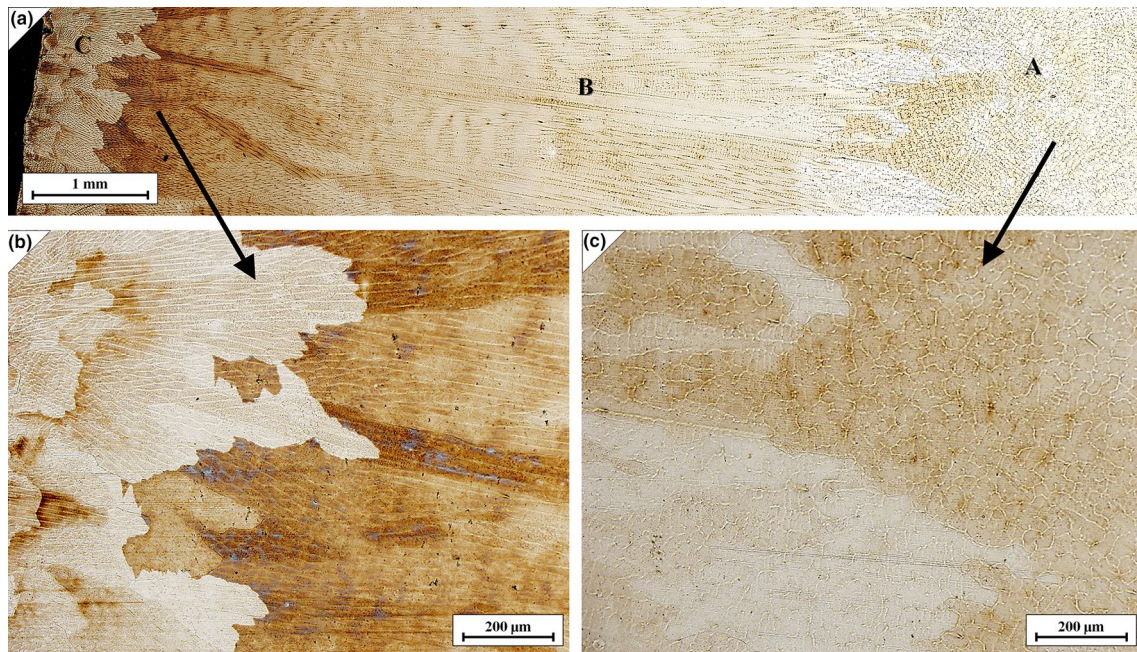
Fig. 8 OM micrographs of primary microstructure of Co–9Al–9W alloy solidified in graphite mold
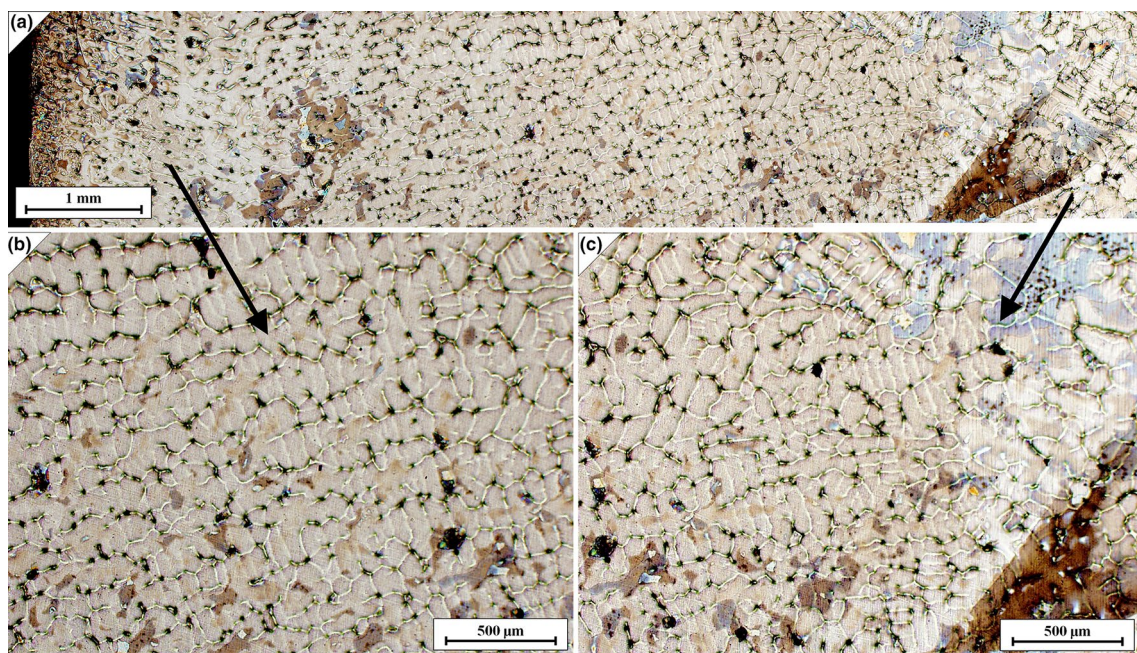

Fig. 9 OM micrographs of primary microstructure of Co–9Al–9W alloy solidified in sand mold

not affect the microstructure and quality of the ingot negatively. Moreover, in the case of crystals' morphology, slow cooling conditions resulted in more beneficial microstructure. Within whole cross section, the crystals were characterized by equiaxial morphology, which is substantially more beneficial compared to that of rapid crystallization. Such

tendency was confirmed at different ingot heights. Further decrease in cooling rate should result in similar effect; however, increase in crystals' size is expected. The morphology of crystals obtained during slow crystallization is favorable from technological point of view. It allows further processing via plastic working, which could be troubling for alloys

Fig. 10 SEM micrographs of primary microstructure of Co–9Al–9W alloy solidified in graphite mold
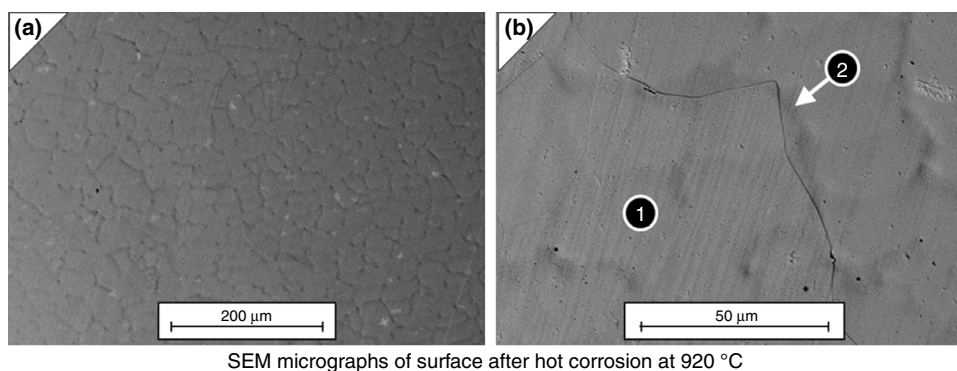
SEM micrographs of surface after hot corrosion at 920 °C

Chemical composition in micro areas marked above

Point	Atom %			Mass		
	Al	Co	W	Al	Co	W
1	6.1	85.5	8.4	2.4	74.6	22.9
2	8.6	83.1	8.4	3.5	73.4	23.1

characterized by dominance of columnar grains. Furthermore, Co-based alloys maintain the morphology of grains after heat treatment. Therefore, such microstructure is also beneficial taking into account the application of cast alloy after precipitation hardening, especially under conditions of high mechanical load.

Furthermore, another considerable finding of casting under low solidification rate is phase composition. The lower crystallization time as well as elongated time of cooling of alloy in solid state may result in precipitation of detrimental phase, e.g., compounds characterized by $D0_{19}$ structure. However, the X-ray diffraction analysis as well as SEM/EDS characterization showed that no unexpected phases occurred. The lack of unfavorable phases was confirmed by X-ray diffraction analysis, SEM/EDS characterization and DTA analysis. Furthermore, increase in crystallization time did not result in excessive segregation of chemical composition, and in formation of detrimental eutectics. All these advantages imply possibility to cast substantially greater elements made of Co–Al–W alloys without risk of unbeneficial structural effects, which is important in view of manufacturing processes.

The solidification path was comparable to that of alloy solidified under rapid heat dissipation and was characterized by two thermal analysis techniques. One of them showed primary crystallization behavior of the alloy. This technique showed temperature window between start and finish of crystallization, which could not be observed precisely on DTA curves. This temperature window is 50 °C, which is relatively thin. Such value should be taken into account in the case of casting parameters selection, especially in the case of manufacturing of components characterized by complex shape. The complex shape of model connected with

unsatisfactory technological parameters (e.g., casting temperature) may result in formation of casting defects, including misrun.

Conclusions

Thermal analysis and microstructural evaluation confirmed that solidification path for Co–Al–W alloy is $L \rightarrow L_1 + \gamma \rightarrow \gamma$. The investigated alloy was characterized by the narrow solidification range, and the difference between the start and end of crystallization was roughly 50 °C.

The primary microstructures of alloy casted under different heat dissipation rates were characterized by dendritic structure. In the case of a rapid crystallization (in graphite mold), the ingot's microstructure was mostly composed of elongated columnar crystals. On the other hand, the microstructure of sand cast was characterized by higher size of dendritic structures, and the structure was beneficial owing to dominance of equiaxed crystals.

For Co–Al–W alloy solidified with different cooling rates, the segregation of Al and W in interdendritic areas was weak. The W-segregation was negligible, whereas the interdendritic areas were slightly enriched in Al.

Acceptable level of segregation and lack of detrimental phases in the primary microstructure, especially in the case of sand cast, imply possibility to produce massive castings made of alloys based on Co–Al–W system.

References

1. Lee CS. Precipitation-hardening characteristics of ternary cobalt–aluminum–X alloys. Arizona: University of Arizona; 1971.
2. Sato J, Omori T, Oikawa K, Ohnuma I, Kainuma R, Ishida K. Cobalt-base high-temperature alloys. Science. 2006;312:90–1.
3. Omori T, Oikawa K, Sato J, Ohnuma I, Kattner UR, Kainuma R, Ishida K. Partition behavior of alloying elements and phase transformation temperatures in Co–Al–W-base quaternary systems. Intermetallics. 2013;32:274–83.
4. Xue F, Zhou HJ, Ding XF, Wang ML, Feng Q. Improved high temperature γ′ stability of Co–Al–W-base alloys containing Ti and Ta. Mater Lett. 2013;112:215–8.
5. Suzuki A, Pollock TM. High-temperature strength and deformation of γ/γ′ two-phase Co–Al–W base alloys. Acta Mater. 2008;56:1288–97.
6. Shinagawa K, Omori T, Sato J, Oikawa K, Ohnuma I, Kainuma R, Ishida K. Phase equilibria and microstructure on γ′ phase in Co–Ni–Al–W system. Mater Trans. 2008;49:1474–9.
7. Yan H-Y, Vorontsov VA, Dye D. Effect of alloying on the oxidation behaviour of Co–Al–W superalloys. Corros Sci. 2014;83:382–95.
8. Meher S, Yan H-Y, Nag S, Dye D, Banerjee R. Solute partitioning and site preference in γ/γ′ cobalt-base alloys. Scr Mater. 2012;67:850–3.
9. Yan H-Y, Vorontsov VA, Dye D. Alloying effects in polycrystalline γ′ strengthened Co–Al–W base alloys. Intermetallics. 2014;48:44–53.
10. Bocchini PJ, Sudbrack CK, Noebe R, Dunand DC, Seidman DN. Microstructural and creep properties of boron- and zirconium-containing cobalt-based superalloys. Mater Sci Eng A. 2017;682:260–9.
11. Rhein RK, Callahan PG, Murray SP, Stinville J-C, Titus MS, Van der Ven A, Pollock TM. Creep behavior of quinary γ′-strengthened Co-based superalloys. Metall Mater Trans. 2018;49:4090–8.
12. McDevitt ET. Vacuum induction melting and vacuum arc remelting of Co–Al–W-X gamma-prime superalloys. In: MATEC web of conferences, vol 14; 2014. p. 02001.
13. Zhong XK, Wang XF, Si YL, Han FS. Evolution of microstructures and properties of a new γ/γ′ Co-based superalloy via forging process. JOM. 2019;71:4034–40.
14. Koßmann J, Zenk CH, Lopez-Galilea I, Neumeier S, Kostka A, Huth S, Theisen W, Gökken M, Drautz R, Hammerschmidt T. Microsegregation and precipitates of an as-cast Co-based superalloy—microstructural characterization and phase stability modelling. J Mater Sci. 2015;50:6329–38.
15. Zhou X, Fu H, Zhang Y, Huan X, Xie J. Effect of Ta and Ti on the solidification characteristics of novel γ′-strengthened Co-base superalloys. J Alloys Compd. 2018;768:464–75.
16. Zhou X, Fu H, Zhang Y, Huan X, Xie J. Effect of Al and W contents on the solidification and solution microstructure of novel γ/γ′ cobalt-base superalloys. Adv Eng Mater. 2019;21:1900641.
17. Sani SA, Arabi H, Kheirandish S, Ebrahimi G. Investigation on the homogenization treatment and element segregation on the microstructure of a γ/γ′-cobalt-based superalloy. Int J Min Met Mater. 2019;26:222–33.
18. Tomaszewska A, Moskal G, Migas D, Mikuśkiewicz M, Maciąg T. Thermal parameters determination of Co–Al–W as-cast alloy homogenization by DTA analysis. J Therm Anal Calorim. 2018;134:157–64.
19. Ding XF, Mi T, Xue F, Zhou HJ, Wang ML. Microstructure formation in γ–γ′ Co–Al–W–Ti alloys during directional solidification. J Alloys Compd. 2014;599:159–63.
20. Tsunekane M, Suzuki A, Pollock TM. Single-crystal solidification of new Co–Al–W-base alloys. Intermetallics. 2011;19:636–43.
21. Kobayashi K, Kainuma R, Fukamichi K, Ishida K. Phase equilibria and stability of B2 and L21 ordered phases in the vicinity of half-metallic composition of Co–Cr–Ga Heusler alloy system. J Alloys Compd. 2005;403:161.
22. Kainuma R, Ohnuma I, Ishida K. Determination of phase diagrams involving order-disorder transitions. In: Zhao J-C, editor. Methods for phase diagram determination. Amsterdam: Elsevier; 2007.
23. Maciąg T, Rzyman K, Przeliorz R. DSC analysis of order–disorder transition in Ni₃Al based alloys from Ni–Al–Cr system. Arch Metall Mater. 2015;60:1871–6.
24. Kazantseva NV, Demakov SL, Yurovskikh AS, Stepanova NN, Vinogradova NI, Davydov DI, Lepikhin SV. Phase diagram of the Co–Al–W system. Structure and phase transformations near the Co₃(Al, W) intermetallic composition range. Phys Met Metallogr. 2016;117:701–9.